PRELIMINARY DESIGN OF LOW LUNAR ORBITS

Martin Lara[(1)], **Bernard De Saedeleer**[(2)], **Sebastián Ferrer**[(3)]

[(1)]*Real Observatorio de la Armada, ES-11110 San Fernando, Spain*
+34 956 545 612, mlara@roa.es

[(2)]*Redu Space Services S.A., B-6890 Redu, Belgium*
+32 (0)61 229 669, bdsa@skynet.be

[(3)]*Dep. Matemática Aplicada, University of Murcia, ES-30071 Espinardo, Spain*
+34 968 367 298, sferrer@um.es

ABSTRACT

The higher order effects of a full lunar gravitational field on the dominating forces on a spacecraft in the vicinity of the moon are investigated. The long term behavior becomes apparent after a first order averaging that removes the spacecraft's mean anomaly and argument of the node. Recurrence equations for the averaged flow in the eccentricity and the argument of perilune are built upon prior recurrences by one of the authors that avoid the need of computing quadratures. Zeros of the reduced flow, which are easily found by means of root-finding procedures, represent higher-order solutions to the frozen orbit problem. These frozen orbits have the argument of perilune either at 90 or 270 deg., depending on inclination, and may hold low eccentricities. Having available analytical equations, the computation of frozen orbits' eccentricity–inclination diagrams is almost inexpensive, and reveals the minimum eccentricity orbits commonly required in preliminary mission design.

1. INTRODUCTION

There is a renewed interest in missions to the moon with a variety of ongoing or proposed missions, including the return of humans for extended stays [1, 2, 3, 4, 5, 6]. New requirements such as lunar satelite communications allowing for permanent south pole coverage, challenge mission designers in the search for frozen orbit architectures that provide long-lifetime orbits in the vicinity of the moon [7, 8, 9, 10].

For higher altitudes than 750 km, operational experience has shown that Earth perturbations dominate the dynamics [8], which can be described with very simple analytical models based on averaging. For lower altitudes, the highly non-spherical lunar gravity field has a notorious effect on the dynamics [11, 12, 13, 14], and full potential models are required for giving a correct description of the motion of low lunar orbiters, even a qualitative one [15, 16, 9, 17].

The derivation of analytical equations for orbit perturbations centered at the moon needs averaging full potentials and the following computation of the averaged flow. But this kind of averaging requires to handle very large expressions formally, and, as a rule, is a priori discarded for general use in preliminary space mission design. However, recent results show that the extensive algebraic manipulations demanded by perturbation methods and the manipulation of resulting huge expressions admit dramatic simplifications in the case of high-inclination orbits. For the specific

case of almost polar orbits, an analytical model that considers fifty zonal gravitational harmonics in addition to the Earth perturbation has been proved to yield the required insight for preliminary mission design [17]. The theory demonstrates the secular drifts in the eccentricity and argument of pericenter due to the third-body and nonspherical gravity perturbations, and reveals as an useful tool for finding (polar or almost polar) frozen orbits.

We extend the theory of Ref. [17] to orbits at any inclination, where simplified potentials are no longer allowed to alleviate computations. However, the averaging process can be avoided because generic analytical recurrences that provide the averaged terms of the perturbing potential for any number of zonal harmonics have been recently derived [18]. The only burden that remains is the size of the formal expressions to handle, but managing large amounts of information is routine for modern computers and software. Besides, there is not need of printing these large formulas to get the required insight, and the formal expressions are safely allocated in few megabytes of memory to be evaluated at will.

The perturbation model consists of a high degree (50×0) lunar gravitational field superimposed on the Earth-moon Hill problem. To the known recurrences in the literature that give the first order, zonal, averaged Hamiltonian, we add new recurrence relations for computing the reduced flow in the eccentricity and the argument of the pericenter, which we use in the search for frozen orbits. We find that the frozen orbits of interest always have an argument of the perilune fixed either at 90 or 270 degrees. Therefore, the frozen orbit computation problem is reduced to a simple one dimensional root-finding problem in the eccentricity for each of these arguments of the perilune.

Because the analytical theory is computed once and for all, we may repeat the search for frozen orbits for a variety of inclinations and, hence, produce the frozen orbits' eccentricity–inclination diagrams that are so useful in preliminary mission design. These kind of diagrams may reveal "critical" inclinations or regions where frozen orbits do not exist, or dips in eccentricity corresponding to almost circular frozen orbits. In addition, contour plots of the averaged perturbing function may be depicted in the form of eccentricity vector diagrams, from which the stability of a given frozen orbit can be assessed. Therefore, by simple inspection of the diagrams produced by the almost inexpensive evaluation of the analytical theory, one can get a general view of the frozen orbits problem and find lunar orbits with usable mission parameters that reduce the need for stationkeeping.

Finally, long-term propagations of selected frozen orbits of our theory show that they remain frozen in the non-averaged model. Besides, we test the reliability of our averaging by comparing our solutions with previous results based on periodic orbits computation on non-averaged full potentials [9]. Thus, starting from the averaged values of the semimajor axis and inclination of a variety of given repeat ground-track, low altitude orbits of the moon, we compute corresponding frozen orbits within the frame of our theory. The agreement between frozen orbit's mean elements and periodic orbits' averaged elements is quite impressive and, in our opinion, supports the validity of the analytical theory.

2. DYNAMICAL MODEL AND AVERAGING

In a planetary satellite system, the motion of a spacecraft around the satellite can be described using Hamiltonian formulation. With an aim of applying perturbation methods, we formulate the problem as a perturbed two-body problem in a rotating frame with constant velocity $\boldsymbol{\nu}$ and with its

origin at the center of mass of the satellite. Thus,

$$\mathcal{H} = (1/2)\,(\boldsymbol{X}\cdot\boldsymbol{X}) - \boldsymbol{\nu}\cdot(\boldsymbol{x}\times\boldsymbol{X}) - (\mu/r) - \mathcal{P}(\boldsymbol{x}) \tag{1}$$

where $\boldsymbol{x} = (x, y, z)$ is the position vector of the orbiter, $r = ||\boldsymbol{x}||$, $\boldsymbol{X} = (X, Y, Z)$ is the vector of conjugated momenta —velocity in the inertial frame, μ is the satellite's gravitational parameter, and the perturbing function $\mathcal{P}$ includes the perturbations of the planet on the spacecraft and the effects due to the non-centrality of the satellite's potential.

The Hamilton equations $\dot{\boldsymbol{x}} = \nabla_{\boldsymbol{X}}\mathcal{H}$, $\dot{\boldsymbol{X}} = -\nabla_{\boldsymbol{x}}\mathcal{H}$, of Eq. (1) give

$$\ddot{\boldsymbol{x}} + 2\boldsymbol{\nu}\times\dot{\boldsymbol{x}} = -\boldsymbol{\nu}\times(\boldsymbol{\nu}\times\boldsymbol{x}) - (\mu/r^3)\,\boldsymbol{x} + \nabla_{\boldsymbol{x}}\mathcal{P}, \tag{2}$$

which are the equations of motion of a nonlinear dynamical system with three degrees of freedom, yet accepting the Jacobi integral $\mathcal{H}(\boldsymbol{X}, \boldsymbol{x}) = C$.

For synchronous orbiting and rotating planetary satellites, equilibrium theory expedites the representation of the satellite by a triaxial ellipsoid with matching orbital and equatorial planes, and with the axes of smaller inertia pointing to the planet. Then, in the Hill problem approximation, the perturbing function is

$$\mathcal{P} = \frac{\nu^2 r^2}{2}\,(3\cos^2\varphi\cos^2\lambda - 1) + \frac{\mu}{r}\sum_{n\geq 2}\left(\frac{\rho}{r}\right)^n \sum_{m=0}^{n}\left(C_{n,m}\cos m\lambda + S_{n,m}\sin m\lambda\right) P_{n,m}(\sin\varphi), \tag{3}$$

where ρ is the equatorial radius of the satellite, $\sin\varphi = u = z/r$, $\tan\lambda = y/x$, $C_{n,m}$, and $S_{n,m}$ are harmonic coefficients, and $P_{n,m}(u)$ are associated Legendre polynomials of degree n and order m.

In the application of this model to the Earth-moon system we neglect the $\pm 5.5\%$ variation in the Earth-moon radius, the ± 8 deg. librations of the moon, and the 5.2 deg. inclination of the moon equatorial plane with respect to its orbital plane.

2.1. Averaged model

The long term dynamics can be studied by averaging the perturbing potential Eq. (3). Due to the small orbital period of an orbiter close to the moon relative to the $\sim$ one month rotation period of the moon, deep tesseral resonances are not expected in general, and a zonal model

$$\mathcal{Z} = \frac{\mu}{r}\sum_{n\geq 2}\left(\frac{\rho}{r}\right)^n C_{n,0}\,P_{n,0}(\sin\varphi) \tag{4}$$

will suffice for studying the secular drifts in the orbital elements produced by the non-sphericity of the central body.

For orbits above, say, few hundred km over the surface of the moon Earth's perturbations dominate the dynamics, and simple analytical expressions can be used to describe the long-term dynamics [7, 8]. Quite on the contrary, higher degree potentials are required for providing a correct description of the motion of low lunar orbiters, even a qualitative one, and the usual claim is that at least 50 zonal harmonics must be retained in the Selenopotential [15, 16, 9]. Averaging potentials of such a high degree requires extensive algebraic manipulations, although dramatic simplifications may be achieved in specific cases [19, 17]. Therefore, the analytical approach is usually discarded for general use in preliminary space mission design of low lunar orbiters. However, at least for

a first-order averaging, straightforward recurrences have been recently established for the direct computation of the averaged zonal potential [18].

To express the perturbing function in orbital elements, we note that

$$\sin\varphi = \sin(f+\omega)\sin I, \qquad r = \frac{a\,\eta^2}{1+e\cos f},$$

where $\eta = \sqrt{1-e^2}$ is the eccentricity function, e the eccentricity, f is the true anomaly, I the inclination, ω the argument of the pericenter and a the semimajor axis. Then, after averaging the mean anomaly ℓ in Eq. (4) one obtains [18],

$$\langle \mathcal{Z} \rangle_\ell = \frac{\mu}{2a} \sum_{n\geq 2} C_{n,0} \left(\frac{\rho}{a}\right)^n \frac{1}{2^{n-1}\eta^{2n-1}}\, \mathcal{S}_n(e,I,\omega)$$

where, calling $n_2 = \mathrm{mod}(n,2)$ that is $n_2 = 0$ for even terms and $n_2 = 1$ for odd terms,

$$\mathcal{S}_n = \sum_{j=n_2}^{n-2} \tilde{\alpha}_{j,n}\, e^j \sum_{i=n_2}^{n} \tilde{\beta}_{i,n}\, \sin^i I \left[\frac{n_2-1}{2}\,\tilde{\gamma}_{i,j,0} + \sum_{k=n_2}^{i} \mathbb{i}^{k-n_2}\,\tilde{\gamma}_{i,j,k}\,\cos(k\,\omega - \tfrac{\pi}{2} n_2) \right] \tag{5}$$

with all three summations going in steps of 2, and the rational coefficients $\tilde{\alpha}_{j,n}$, $\tilde{\beta}_{i,n}$, and $\tilde{\gamma}_{i,j,k}$ are

$$\tilde{\alpha}_{j,n} = \frac{1}{2^j}\binom{n-1}{j}, \qquad \tilde{\beta}_{i,n} = (2\,\mathbb{i})^{n-i}\,\frac{(n-1+i)!!}{(n-i)!!\;i!}, \qquad \tilde{\gamma}_{i,j,k} = 2\binom{i}{\frac{i-k}{2}}\binom{j}{\frac{j-k}{2}}.$$

We use the notation $\mathbb{i} = \sqrt{-1}$ for the imaginary unit, which is always raised to an even number. Note that we introduced slight modifications to De Saedeleer's original formulas for convenience in our computational procedures, and write reordered coefficients with a tilde to stress that they are different from those in [18], a reference which should consult any reader interested in details.

In addition, the third body contribution needs a double averaging to remove also the argument of the node in the rotating frame $h = \Omega - \nu\, t$. The doubly averaged Hill problem is a recurrent model in the Literature since its original proposal [20, 21]. A list of references can be found in [22] where details on the averaging are also provided.

Averaging over h lefts $\langle \mathcal{Z} \rangle_\ell$ unaltered, resulting in the doubly averaged perturbing function

$$\widetilde{\mathcal{P}} = \langle \mathcal{P} \rangle_{\ell,h} = \langle \mathcal{Z} \rangle_\ell + \frac{\mu}{2a}\left(\frac{\nu}{N}\right)^2 \frac{1}{8}\left[(2-3\sin^2 I)\,(2+3e^2) + 15e^2\sin^2 I\cos 2\omega\right], \tag{6}$$

where $N = \sqrt{\mu/a^3}$ is the mean motion of the orbiter, which is constant after averaging, and has been introduced to manifest the relative importance of the third body perturbation. Thus, for orbits close the moon the mean motion is of the order of two hours what makes $(\nu/N)^2 \sim 10^{-5}$, while many of the un-normalized gravitational harmonics of the moon are of the same order.

2.2. Reduced flow: frozen orbits

Better than working with Lagrange planetary equations and orbital elements, we introduce their canonical counterpart: the set of Delaunay elements (L, G, H, ℓ, g, h), where $L = \sqrt{\mu\, a}$ is the Delaunay action, $G = L\sqrt{1-e^2}$ is the modulus of the angular momentum vector, $H = G\cos I$

is its polar component, $g = \omega$ is the argument of the pericenter, and ℓ and h have been already defined as the mean anomaly and the argument of the node in the rotating frame, respectively.

Because ℓ and h are cyclic in the averaged Hamiltonian

$$\widetilde{\mathcal{H}} = \langle \mathcal{H} \rangle_{\ell,h} = -\frac{\mu^2}{2L^2} - \nu\, H - \widetilde{\mathcal{P}}(g, G; L, H), \tag{7}$$

L and H are integrals of the averaged motion, and the reduced flow in (G, g)

$$\dot{g} = \frac{\partial \widetilde{\mathcal{H}}}{\partial G} = -\frac{\partial \widetilde{\mathcal{P}}}{\partial G}, \qquad \dot{G} = -\frac{\partial \widetilde{\mathcal{H}}}{\partial g} = \frac{\partial \widetilde{\mathcal{P}}}{\partial g}, \tag{8}$$

decouples from the other Hamilton equations.

The reduced flow, Eq. (8), is of one degree of freedom and, therefore, integrable; once it has been integrated, the secular evolution of ℓ and h can be obtained by quadratures

$$\ell = \ell_0 + N\, t - \int \frac{\partial}{\partial L} \widetilde{\mathcal{P}}(g(t), G(t); L, H)\, \mathrm{d}t, \qquad h = h_0 - \nu\, t - \int \frac{\partial}{\partial H} \widetilde{\mathcal{P}}(g(t), G(t); L, H)\, \mathrm{d}t.$$

The analytical solution of the averaged flow is made of huge expressions that involve elliptic and hyper-elliptic integrals, therefore, providing poor insight, if any, on the averaged dynamics. Then, instead of trying to find the analytical solution to the averaged problem, we better pay attention only to particular solutions of interest in astrodynamics. Specifically we focus on the equilibria of the reduced flow $\dot{G} = \dot{g} = 0$. These solutions correspond to orbits that, on average, remain with constant eccentricity and inclination, and with fixed argument of pericenter, which are called frozen orbits (see [23] for a large list of references on the topic).

Recurrences for constructing the time derivative of G are trivial from Eq. (5), because it only implies changing sines by cosines and vice-versa, besides the introduction of corresponding factors. On the contrary, the time derivative of g is much more involved. However, after some manipulation, one finds that the recurrences are strikingly similar to those of the Hamiltonian. Thus,

$$\dot{g} = N \left(\frac{\nu}{N}\right)^2 \frac{3}{8\eta} \left[4\eta^2 + 5(e^2 - \sin^2 I)\,(1 - \cos 2g)\right] + N \sum_{n\geq 2} C_{n,0} \left(\frac{\rho}{a}\right)^n \frac{\mathcal{S}_n^\star(e, I, g)}{2^n\, \eta^{2n}}, \tag{9}$$

where the $\mathcal{S}_n^\star$ are constructed from corresponding $\mathcal{S}_n$ by simply changing the coefficients $\tilde{\beta}_{i,n}$ by the new functions $\Psi_{i,j,n}(e, I)$ that are given by

$$\Psi_{i,j,n} = \left(1 + j - i - 2n + \frac{i}{\sin^2 I} - \frac{j}{e^2}\right) \tilde{\beta}_{i,n}. \tag{10}$$

We note that $\dot{G} \equiv 0$ for $g = \pm\pi/2$. Therefore, the search for frozen orbits with the pericenter either at 90 or 270 deg. reduces to a one dimensional, root-finding problem in G in Eq. (9) where $\dot{g}(g = \pm\frac{\pi}{2}, G; L, H) = 0$. Once G is solved, the frozen orbit's eccentricity and inclination are easily computed from $e = \sqrt{1 - G^2/L^2}$, and $\sin I = \sqrt{1 - H^2/G^2}$.

Alternatively, taking advantage of the fact that Eq. (9) is expressed in orbital elements, the frozen orbits, root-finding problem can be solved directly in the eccentricity for a given inclination. In fact, we only need to deal with one of the cases $g = \pm\pi/2$. Indeed, the third body contribution to Eq. (9) depends on $\cos 2g$ that evaluates to -1 for $g = \pm\pi/2$. Besides, we note in Eq. (5),

and in its starred analog, that for n even, cosines in the argument of the pericenter just evaluate to the same expression: plus ore minus one for $g = \pm\pi/2$, whereas e is always raised to even powers. Alternatively, for n odd, sine functions in the argument of the pericenter in Eq. (5), and in its starred analog, change their value from ± 1 to ∓ 1 when the argument of the pericenter switches from $g = \pi/2$ to $g = -\pi/2$, whereas e is always raised to odd powers. Therefore, we see that orbits with frozen pericenter at $\pm\pi/2$ may be computed from a numeric root-finding in Eq. (9) for the single value $g = \pi/2$ but allowing for "negative" e values, which correspond to the case $-e = e\sin(-\pi/2)$.

The numerical search can be made by standard methods, but paying special attention to the numerical errors because of the large number of terms involved. Thus, for instance, the Newton-Raphson approach:

$$e_{m+1} = e_m - \frac{\dot g(e_m)}{\partial \dot g(e_m)/\partial e_m},$$

besides the evaluation of $\dot g$ requires the evaluation of

$$\begin{aligned}\frac{\partial \dot g}{\partial e} &= N\left(\frac{\nu}{N}\right)^2 \frac{3e}{8\eta}\left[5\frac{\eta^2+\cos^2 I}{\eta^2}\left(1-\cos 2g\right)-4\right]\\ &\quad +N\sum_{n\geq 2} C_{n,0}\left(\frac{\rho}{a}\right)^n \frac{1}{2^n\,\eta^{2n}}\left[\frac{2n\,e}{\eta^2}\,\mathcal{S}_n^\star(e,I,g)+\frac{\partial \mathcal{S}_n^\star(e,I,g)}{\partial e}\right],\end{aligned}$$

with trivial recurrences for the computation of $\partial\mathcal{S}_n^\star/\partial e$, but which roughly doubles the number of terms in $\dot g$.

Other frozen orbits might exist with different arguments of pericenter, the computation of which requires a numerical two dimensional search in (G, g). We did not succeed in finding any of them, at least for the low eccentricities required by non impact, low altitude lunar orbits.

3. RESULTS

Once the necessary formulas have been tuned, we are ready to explore the long term behavior of the orbital elements. In our computations we use a 50×0 truncation of the spherical harmonic representation of the gravity field of the moon, which we extract from the publicly available[1] `lp150q` model [24, 25] —un-normalized n-zonal coefficients are obtained multiplying corresponding normalized ones of the `lp150q` model by the factor $\sqrt{2n+1}$. Besides, in all our simulations we consider the Earth perturbations in the Hill problem approximation. Therefore, in what follows, when we talk about some truncation of the selenopotential it must be always understood that the model also includes the third-body perturbations.

For given values of the integrals L and H of the averaged problem, or $a = L^2/\mu$ and

$$\sigma = H/L = \sqrt{1-e^2}\cos I,$$

we can compute a frozen orbit with g at $\pi/2$ or $-\pi/2$ by making $\dot g = 0$ in Eq. (9) and solving it for G. Alternatively, we can fix the semimajor axis and compute directly the eccentricity of the frozen orbit (with pericenter at plus or minus $\pi/2$) for a given value of the inclination from Eq.

[1] http://pds-geosciences.wustl.edu/geodata/lp-l-rss-5-gravity-v1/lp_1001/sha/jgl150q1.sha

(9) as described above. By repeating the procedure for all the range of inclinations of interest, we obtain the eccentricity-inclination diagrams that are so illustrative in preliminary mission design.

Figure 1 shows an eccentricity-inclination diagram of frozen orbits with a mean semimajor axis $a = 1861$ km (the same semimajor axis as the 30×216 km quasi-frozen orbit considered for the commissioning period of the Lunar Reconnaissance Orbiter [8]). We choose this semimajor axis because the third-body perturbation starts to be apparent at corresponding altitudes, although the selenepotential clearly dominates the dynamics. As the averaged problem is symmetric with respect to the inclination, which only appears through $\sin$ functions in the Eqs. (6) and (9), we only present the case of direct frozen orbits. In the figure we limit the range of eccentricities to non-impact orbits, which exist for all the range of inclinations except for three gaps in the vicinity of 35, 55, and 65 deg., respectively.

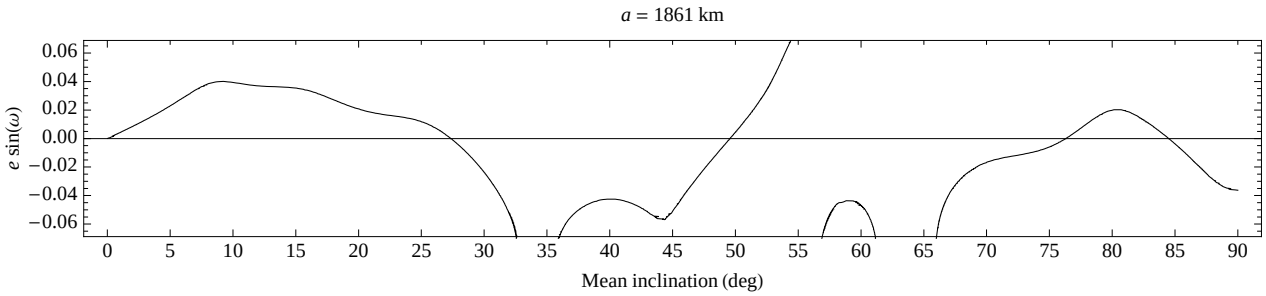

Fig. 1. Lunar frozen orbits eccentricity-inclination diagram (50×0 truncation). The argument of the perilune is restricted to either $\omega = 90$ or $\omega = 270$ deg.

In reference to Fig. 1, starting from polar we find a frozen orbit with the pericenter at $\omega = 270$ deg. and $e \approx 0.04$; the eccentricity decreases with inclination while the pericenter holds until reaching an inclination $I = 84.5$ deg., where we find a circular frozen orbit (mean eccentricity zero). The pericenter of lower inclination frozen orbits switches to $\omega = 90$ deg., and the eccentricity increases until a frozen orbit impacts the moon at $I = 66.4$ deg. ($e = 0.066$). We do not find more non-impact forzen orbits until the inclination reduces to $I = 60.8$ deg. The frozen orbits become impact orbits again at $I = 57.2$ deg. After a new gap of about 3 deg. of inclination, we find new non-impact frozen orbits for inclinations below $I = 54$ deg., but now the pericenter is at $\omega = 90$ deg. A new circular frozen orbit is found with $I = 49.6$ deg. For lower inclinations the pericenter changes to $\omega = 270$ deg. and the eccentricity grows. A new impact frozen orbit is found at $I = 36.4$ deg. Non-impact frozen orbits exist again for $I < 32.3$ deg. with a circular one at $I = 24.4$ deg.; at this point the pericenter switches again to $\omega = 90$ deg. and remains there for lower inclinations.

It remains to check the stability of specific solutions. Since Eq. (8) is a differential system of one degree of freedom, the reduced flow is made only of equilibria and closed curves. Stable equilibria are elliptic points of the flow, and unstable equilibria are hyperbolic points. Therefore, the stable or unstable character of the computed frozen orbits (equilibria of the reduced flow) should be obtained from the graphic representation of the flow, which can be done in the form of eccentricity vector diagrams. These diagrams can be constructed without need of integrating Eq. (8), by simple evaluation of the averaged perturbing function, Eq. (6), as indicated below (see also [26]).

For given values of the integrals L and H of the averaged problem (or a and σ), the perturbing function is constant on average; say $\widetilde{\mathcal{P}}(G, g; L, H) = P_0$. If the averaged perturbing function is

written in terms of the semi-equinoctial elements $q = e\cos g$, $p = e\sin g$, then, contour plots of $\widetilde{\mathcal{P}}(q, p; a, \sigma)$ for different values of P_0 will provide the desired eccentricity vector diagram.

We illustrate the procedure by computing several of these eccentricity vector diagrams for the value $a = 1861$ km. We choose the values of the parameter σ corresponding to the frozen orbits detailed in Table 1. Then, contour plots of the averaged perturbing function for each pair (a, σ) are computed for the range of non-impact orbits. Results are shown in Fig. 2.

Table 1: Lunar frozen orbits with mean semimajor axis $a = 1861$ km. S stands for stable and U for unstable

σ	0.9841	0.7061	0.5870	0.5144	0.3904	0.1736
e	0.0388	0.0537	0.0530	0.0504	0.0440	0.0177
I deg.	10	45	54	59	67	80
ω deg.	90	270	90	270	270	90
Stability	S	S	S	U	S	S

The stability behavior of the frozen orbits on Table 1 is easily appreciated in the plots of Fig. 2. At the altitudes corresponding to the selected semimajor axis $a = 1861$, we find that lunar frozen orbits are generally stable. The stable behavior manifests by the ellipses surrounding the fixed points in most of the plots of Fig. 2. But we also find unstable behavior for inclinations between $I = 57.2$ and $I = 60.8$ deg., conform the eccentricity vector diagram in the center right plot of Fig. 2, where the reduced flow clearly shows the hyperbolic character of the fixed point (frozen orbit).

To stress the important variations in the behavior of frozen orbits when lower degree truncations of the Selenopotential are considered, we compute similar eccentricity-inclination diagrams for a 20×0 and a 7×0 truncations of the selenopotential. Results are presented in Fig. 3. While the 20×0 truncation (dotted line) shows a similar qualitative behavior to the 50×0 one (full line), the aproximation is only acceptable for medium and low inclination orbits. For higher inclination orbits the 20×0 truncation only approximates roughly the 50×0 case, giving frozen orbits that, in general, show lower eccentricities, and shifting the zero eccentricity solutions to lower inclinations by several degrees. Even worse is the case of the 7×0 truncation of the selenopotential (dashed line of Fig. 3), which provides a correct qualitative description only in the case of low inclinations. For medium and high inclination frozen orbits the behavior of the 7×0 truncation is clearly different from the other truncations, not only for the notably different evolution of the eccentricity values, but for it also provides a completely wrong argument of the periapsis in many cases.

For orbits at higher altitudes, the harmonics of higher degree have a lesser influence and the gravitational model can certainly be simplified. Thus, for instance, for orbits about 300 km over the surface of the moon the 20×0 truncation may be enough for describing the long term dynamics of the lowest eccentricity frozen orbits. However, as Fig. 4 shows, the 7×0 truncation still provides a wrong behavior for high inclination orbits. From our computations, we find that the 7×0 truncation of the selenopotential starts to be an acceptable model for low-eccentricity orbits that remain above, say, 600 km over the surface of the moon.

Comparison with periodic solutions of the non-averaged problem provides a further test on the correctness of the analytical approach. To this effect we use results computed in [9]; specifically, we deal with the family of 328-cycle repeat ground-track orbits computed for the same, 50×0

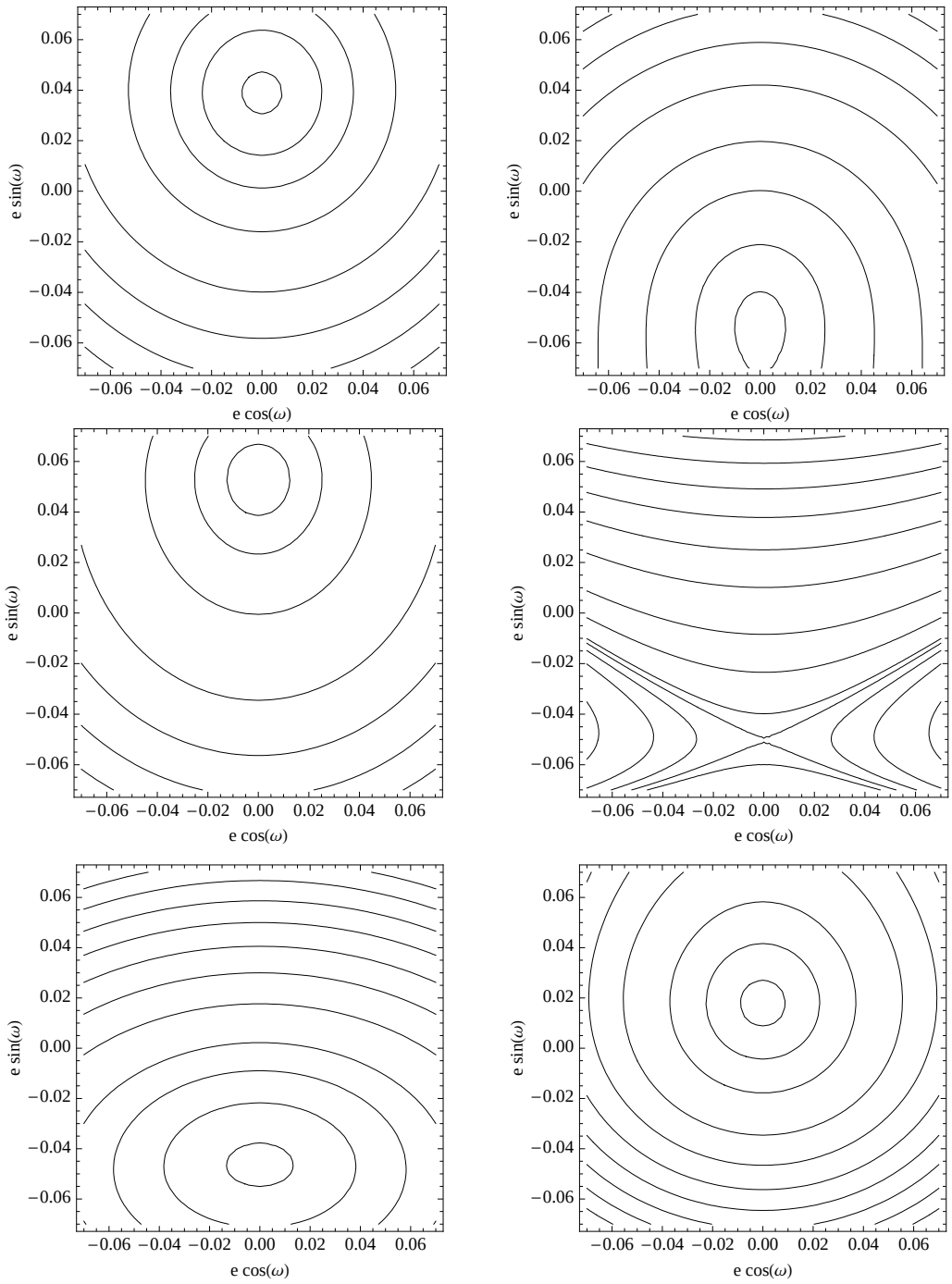

Fig. 2. Eccentricity vector diagrams of lunar orbits with $a = 1861$ km and: $\sigma = 0.9841$, top left, $\sigma = 0.7061$, top right, $\sigma = 0.5870$, center left, $\sigma = 0.5144$, center right, $\sigma = 0.3904$, bottom left, and $\sigma = 0.1736$, bottom right.

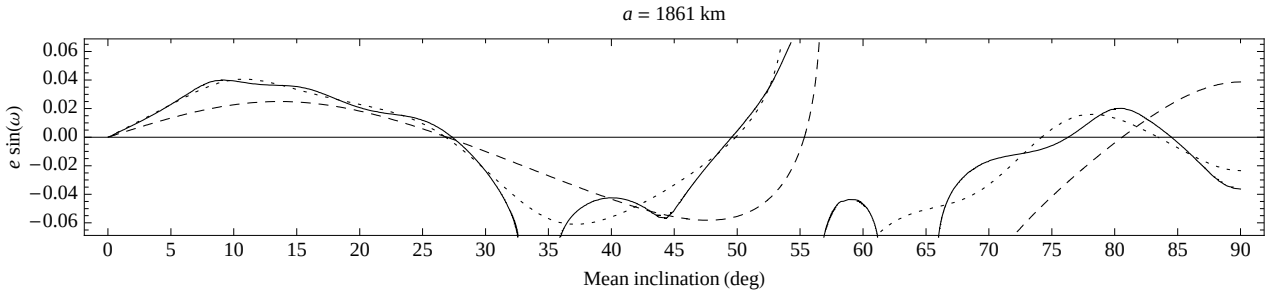

Fig. 3. Lunar frozen orbits: 50×0 (full line), 20×0 (dotted), and 7×0 (dashed) truncations of the selenopotential. The argument of the perilune ω is restricted to either 90 or 270 deg.

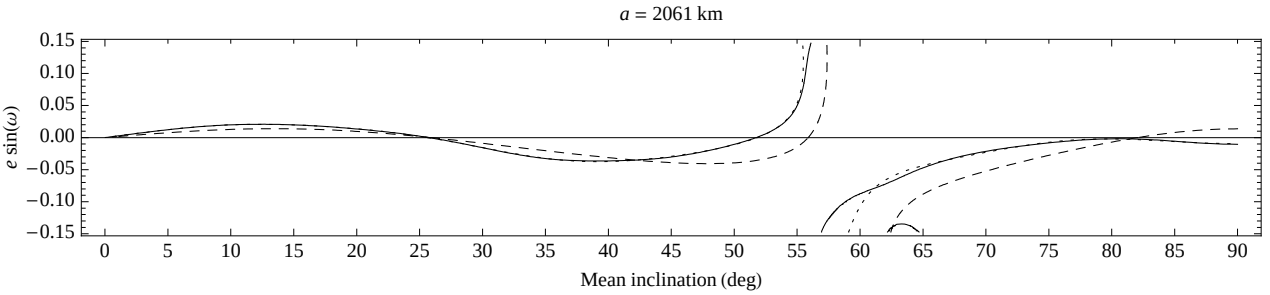

Fig. 4. Lunar frozen orbits: 50×0 (full line), 20×0 (dotted), and 7×0 (dashed) truncations of the selenopotential. The perilune is at either $\omega = 90$ or $\omega = 270$ deg.

truncation of the selenopotential, although the Earth perturbation was modeled in [9] using the circular restricted three-body problem instead of the Hill's simplification. This difference in the model introduces negligible effects in the low altitude orbits we deal with in the present study.

Figure 5 shows a direct comparison between the lunar 328-cycle family of periodic orbits and our family of frozen orbits with mean semimajor axis $a = 1861$ km. The qualitative agreement is good, but we note that the direct comparison is not quite correct because, whereas the mean semimajor axis of the computed frozen orbits remains constant, the semimajor axis of the repeat-ground track orbits must change with inclination to maintain periodicity. And it does vary between 1808 and 1903 km for the chosen example, as shown by the dashed line on Fig. 5 going from the left-down to the top-right corners of the plot. The change in semimajor axis is what produces the non-symmetric behavior of the eccentricity of direct and retrograde inclination orbits. In addition, frozen orbits are quasi-periodic solutions of the non-averaged problem that do not need to be periodic neither on average or in the non-averaged problem.

We carry out a more consistent comparison by computing a frozen orbit for each semimajor axis and inclination of the corresponding repeat-ground track orbit. The new results are presented in Fig. 6, where we now note the perfect agreement between the mean elements predicted by the analytical theory and average elements of the periodic orbits of the non-averaged model.

We perform several further tests to asses the degree of correction of the analytic theory in quantitative terms. To this effect, we transform the frozen orbit's mean elements provided by the analytic theory directly into initial conditions, and propagate them in the non-averaged model. Thus, Fig. 7 shows a long term propagation of a frozen orbit with mean elements $a = 1861$ km, $e = 0.0036$, $I = 84$ deg., and $g = 90$ deg.; the initial conditions were computed for $\ell = h = 0$. After three years, the orbit remains frozen with elements that average to $a = 1861.6$ km, $e = 0.0041$, $I = 83.94$ deg., and $\omega = 92.36$ deg.; the perilunar distance averages to 115.88 km, and the

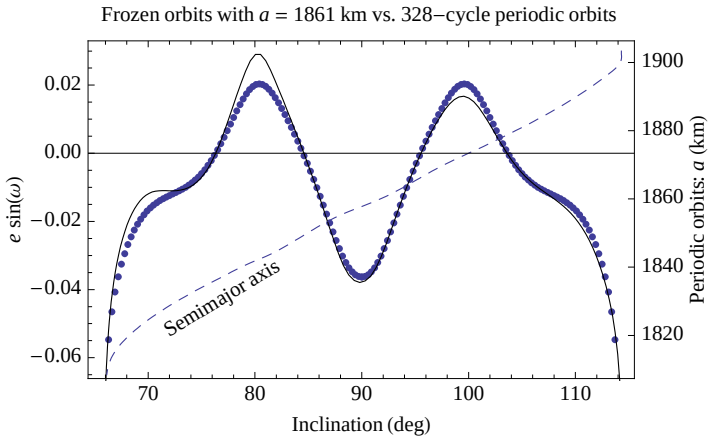

Fig. 5. Frozen (dots) vs. periodic orbits (full line) evolution with inclination (50×0 truncation). ω is either 90 or 270 deg.

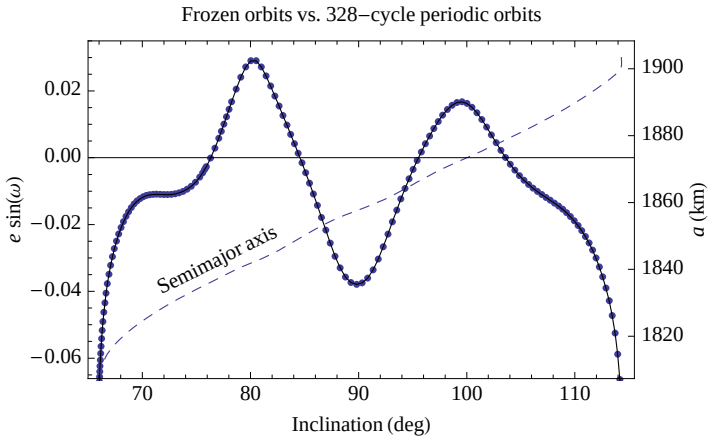

Fig. 6. Frozen (dots) vs. periodic orbits (full line) with the same semimajor axis and inclination (50×0 truncation). ω is either 90 or 270 deg.

node rate is of ~ 0.12 deg./day.

The orbit indeed remains frozen, but it is still affected of small amplitude, long period effects of about two years. Besides, medium period effects due to the third body perturbations, missed in the averaging, are apparent in the propagation to show weekly oscillations with an amplitude less than one thousand in eccentricity, 25 deg. in the argument of the perilune, and of ± 0.5 km in the semimajor axis. Semimonthly oscillations of 0.13 deg. in inclination are also observed.

Lower eccentricity orbits in the long term may be obtained from frozen orbits with zero mean eccentricity, however they result in circulating perilune in the non averaged problem. Figure 8 shows the evolution of some orbital elements in a three year propagation of the frozen orbit with mean elements $a = 1861$ km, $e = 0.0007$, $I = 84.6$ deg., $g = 270$ deg., $\ell = h = 0$. As observed in the figure, the osculating eccentricity remains with very low values, always below one thousandth.

Another worthy test on the reliability of the theory is the computation of the unstable frozen orbit in the center right plot of Fig. 2, because this orbit is not apparent in lower order theories, cf. Fig. 3. We compute initial conditions from mean elements $a = 1861$ km, $e = 0.04268$, $I = 59.1$ deg., $g = 270$ deg., $\ell = h = 0$, and launch a three years propagation. Results are shown

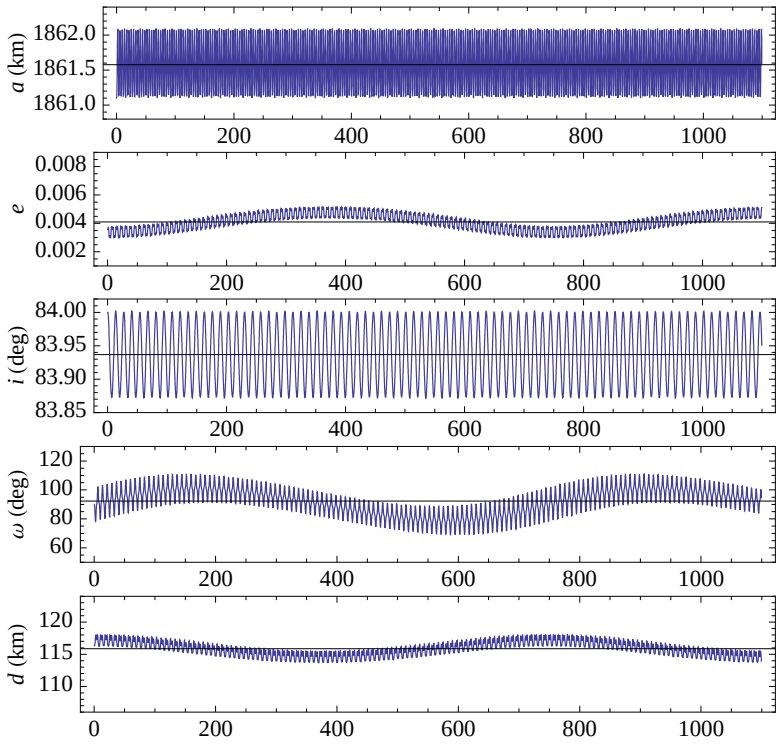

Fig. 7. Osculating elements and periselene distance d of the frozen orbit of Fig. 1 with mean inclination $I = 84$ deg. Abscissas are days.

in Fig. 9, where we note that the orbit remains with constant orbital elements, on average, for more than one year; then, it derails over the unstable manifold: the eccentricity grows high and, if left uncontrolled, the orbiter impacts the moon after 2.8 years with an argument of the perilune $\omega = 237$ deg.

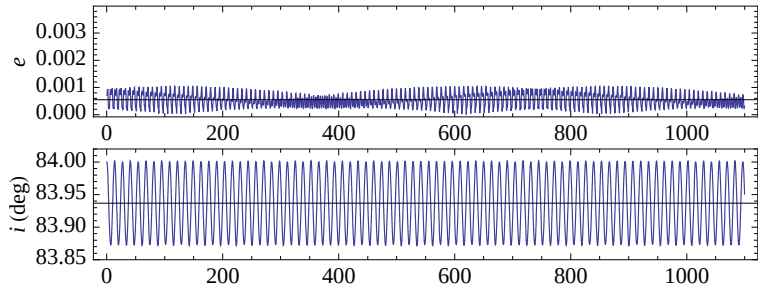

Fig. 8. Osculating eccentricity and inclination of the almost circular frozen orbit of Fig. 1 with mean inclination $I = 84.6$ deg. Abscissas are days.

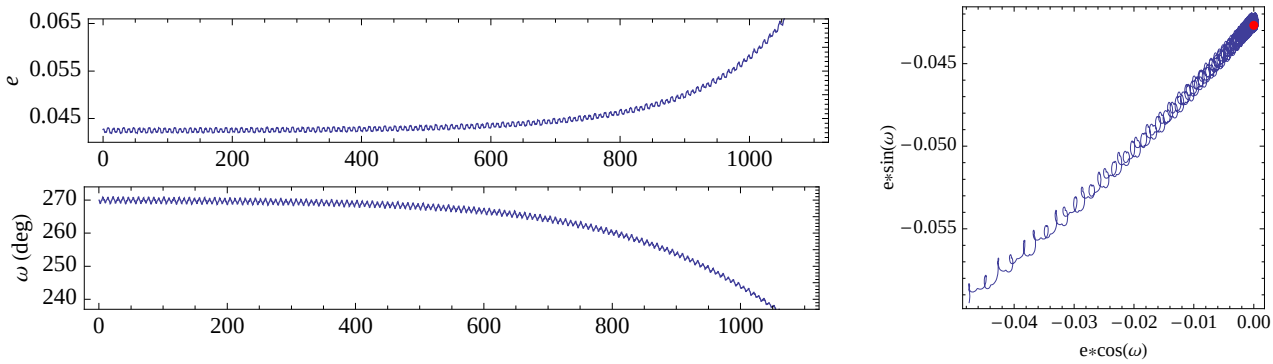

Fig. 9. Unstable, frozen orbit of Fig. 1 with mean inclination $I = 59.2$ deg. Left: Osculating elements; abscissas are days. Right: eccentricity vector diagram.

4. CONCLUSIONS

With the current state of computational power, high degree potential models can be handled formally without major difficulties, a fact that provides new views on how to face up to orbit design problems since the preliminary stages. This is of particular relevance in the case of the moon, where the orbit behavior is highly influenced by the distribution of the lunar mascons and Earth perturbations, and high fidelity potential models are required to capture the dynamics of orbiters close to its surface.

For the gravity field of the moon, the present analytical study demonstrates the existence of low-eccentricity frozen orbits in all the range of inclinations. These frozen orbits are generally stable, and may enjoy very low eccentricities at a handful of specific inclinations. The averaged dynamics gives a qualitative description of the long term behavior of low lunar orbits, but it also provides accurate enough initial conditions to be used in the non averaged model.

Our study considers perturbations from the Earth in the Hill problem approximation, and is based on a 50×0 truncation of the `lp150q` lunar gravitational model. However, since the theory has been computed fully analytically, there will be no additional effort in updating the gravity field with the improved values that should soon become available from a variety of missions like the Japanese SELENE, the Chinese Chang'e-1, the Indian Chandrayaan-1, or the recent NASA Lunar Reconnaissance Orbiter.

Acknowledgements

Partial support to perform this research comes from Projects ESP 2007-64068 (M.L) and MTM 2006-06961 (S.F.) of the Government of Spain, and from a grant of Fundación Séneca of the Autonomous Region of Murcia (S.F. and M.L.).

References

[1] Kato, M., Sasaki, S., Tanaka, K., Iijima, Y., and Takizawa, Y., "The Japanese lunar mission SELENE: Science goals and present status," *Advances in Space Research*, Vol. 42, No. 2, 2008, pp. 294-300.

[2] Huixian, S., Shuwu, D., Jianfeng, Y., Ji, W., and Jingshan, J., "Scientific objectives and payloads of Chang'E-1 lunar satellite," *Journal of Earth System Science*, Vol. 114, No. 6, 2005, pp. 789-794.

[3] Bhandari, N., "Chandrayaan-1: Science goals," *Journal of Earth System Science*, Vol. 114, No. 6, 2005, pp. 701-709.

[4] Chin, G., Brylow, S., Foote, M., Garvin, J., Kasper, J., Keller, J., Litvak, M., Mitrofanov, I., Paige, D., Raney, K., Robinson, M., Sanin, A., Smith, D., Spence, H., Spudis, P., Stern, S.A., and Zuber, M., "Lunar Reconnaissance Orbiter Overview: The Instrument Suite and Mission," *Space Science Reviews*, Vol. 129, No. 4, 2007, pp. 391-419.

[5] *The Vision for Space Exploration*, National Aeronautics and Space Administration Publication, NP-2004-01-334-HQ, 2004.

[6] *2006 NASA Strategic Plan*, National Aeronautics and Space Administration Publication, NP-2006-02-423-HQ, 2006.

[7] Ely, T.A., "Stable Constellations of Frozen Elliptical Inclined Lunar Orbits," *Journal of the Astronautical Sciences*, Vol. 53, No. 3, 2005, pp. 301-316.

[8] Folta, D., and Quinn, D., "Lunar Frozen Orbits," Paper AIAA 2006-6749, August 2006.

[9] Russell, R.P., and Lara, M., "Long-Lifetime Lunar Repeat Ground Track Orbits," *Journal of Guidance, Control, and Dynamics*, Vol. 30, No. 4, 2007, pp. 982-993.

[10] Howell, K.C., Grebow, D.J., and Olikara, Z.P., "Design Using Gauss' Perturbing Equations with Applications to Lunar South Pole Coverage," Paper AAS 07-143, February 2007.

[11] Cook, R.A., and Sweetser, T.H., "Orbit Maintenance for Low-Altitude Near-Circular Lunar Orbits," Paper AAS 92-185, February 1992.

[12] Meyer, K.W., and Buglia, J.J., Desai, P.N., "Lifetimes of Lunar Satellite Orbits," NASA Technical Paper 3394, March 1994.

[13] d'Avanzo, P., Teofilatto, P., and Uliveri, C., "Long-Term Effects on a Lunar Orbiter," *Acta Astronautica*, Vol. 40, No. 1, 1997, pp. 13-20.

[14] Ramanan, R.V., and Adimurthy, V., "An analysis of near-circular lunar mapping orbits," *Journal of Earth System Science*, Vol. 114, No. 6, 2005, pp. 619-626.

[15] Konopliv, A.S., Sjogren, W.L., Wimberly, R.N., Cook, R.A., and Vijayaraghavan, A., "A High Resolution Lunar Gravity Field and Predicted Orbit Behavior," Paper AAS 93-622, August 1993.

[16] Roncoli, R. B., "Lunar Constants and Models Document," JPL D-32296, Jet Propulsion Laboratory, Pasadena, CA, September 2005, Sec. 2.1.

[17] Lara, M., Ferrer, S., and De Saedeleer, B., "Lunar analytical theory for polar orbits in a 50-degree zonal model," Paper AAS 09-157, February 2009 .

[18] De Saedeleer, B., "Complete zonal problem of the artificial satellite: generic compact analytic first order in closed form," *Celestial Mechanics and Dynamical Astronomy*, Vol. 91, No. 3, 2005, pp. 239-268.

[19] Knežević, Z., and Milani, A., "Orbit maintenance of a lunar polar orbiter," *Planetary and Space Science*, Vol. 46, 1998, pp. 1605-1611.

[20] Lidov, M.L., "The Evolution of Orbits of Artificial Satellites of Planets Under the Action of Gravitational Perturbations of External Bodies," *Planetary and Space Science*, Vol. 9, 1962, pp. 719-759 (Translation from *Iskusstvennye Sputniki Zemli*, No. 8, 1961, pp. 5-45).

[21] Kozai, Y., "Motion of Lunar Orbiter," *Publications of the Astronomical Society of Japan*, Vol. 15, No. 3, 1962, pp. 301-312.

[22] Broucke, R.A., "Long-Term Third-Body Effects via Double Averaging," *Journal of Guidance and Control*, Vol. 24, No. 1, 2003, pp. 27-32.

[23] Coffey, S.L., Deprit, A., and Deprit, E., "Frozen Orbits for Satellites Close to an Earth-like Planet," *Celestial Mechanics and Dynamical Astronomy*, Vol. 59, 1994, pp. 37-72.

[24] Konopliv, A., Asmar, S.W., Carranza, E., Sjogren, W.L., and Yuan D.N., "Recent Gravity Models as a Result of the Lunar Prospector Mission," *Icarus*, Vol. 150, No. 1, 2001, pp. 1-18.

[25] Konopliv, A., "Lunar Prospector Spherical Harmonic Models and Digital Maps," NASA Planetary Data System, LP-L-RSS-5-GRAVITY-V1.0, 1999.

[26] Coffey, S., Deprit, A., Deprit, E., and Healy, L., "Painting the Phase Space Portrait of an Integrable Dynamical System," Science, Vol. 247, No. 4944, 1990, pp. 833-836.